Nanoscale

COMMUNICATION
Danner, Teng, Liu *et al.*
Reflective plasmonic color filters based on lithographically patterned silver nanorod arrays

NCNST

RSCPublishing

Nanoscale

COMMUNICATION

Reflective plasmonic color filters based on lithographically patterned silver nanorod arrays

Guangyuan Si,†[a] Yanhui Zhao,†[b] Jiangtao Lv,[a] Mengqian Lu,[b] Fengwen Wang,[a] Hailong Liu,[c] Ning Xiang,[c] Tony Jun Huang,[b] Aaron J. Danner,*[c] Jinghua Teng*[d] and Yan Jun Liu*[d]

We demonstrate reflection-mode plasmonic color filters based on lithographically patterned silver nanorods with ultrasmall inter-rod gaps. Fine and effective tuning of the plasmon resonance is shown by varying array periodicities. We determine the dependence of reflected intensity on diameter/periodicity ratio and then develop reflective plasmonic color filters using dense nanorod arrays. Experimental results agree well with theoretical calculations. Our approach is potentially useful for plasmon-assisted sensing, imaging and displays.

Introduction

Plasmonics provides the unique capability of manipulating light at sub-wavelength scales by using versatile nanostructures, such as cubes,[1–3] clusters,[4–6] shells,[7,8] disks,[9–11] holes,[12,13] rings,[14,15] rods,[16–20] and particles with arbitrary shapes.[21–23] Many different kinds of plasmonic device have been demonstrated so far, including modulators,[24] interferometers,[25] switches,[26,27] polarizers,[28,29] and absorbers.[30–33] Color filters are an essential component in imaging sensors, color displays, digital cameras, and other related applications. Recently, interest in plasmon-assisted color filters has greatly increased due to their ultracompact design, ultrahigh resolution, and convenient integration. So far, various plasmonic color filters, such as nanoslits with periodical grooves,[34] metal–insulator–metal stacks,[35,36] and annular aperture arrays,[37–39] have been demonstrated. However, most efforts have been concentrated on transmission-mode color filters instead of reflection-mode

ones. Very recently, researchers have shown that it is feasible to control colors using functional "intaglio/bas-relief"[40] or nanodisks with backreflector[41] under reflection mode.

Metallic nanorod arrays with preferred alignment and periodicities are of particular importance for surface plasmon resonances and couplings, hence affecting photon flow accordingly.[42] However, it is very challenging to fabricate a dense nanorod array with ultrasmall gaps and large aspect ratios using normal lift-off methods. In this communication, we fabricate dense silver nanorod arrays with ultrasmall gaps through electron-beam lithography (EBL) followed by ion milling. The effects of periodicity (p) and diameter/periodicity (d/p) ratio of the silver nanorod arrays on the plasmon resonance are investigated. By controlling their geometries, we show that such nanorod arrays are capable of tuning the plasmon resonance and further reflectively filtering out individual colors from a broadband light source. Hence, they can serve as reflective plasmonic color filters, which may find extensive application ranging from color filtering to spectral imaging.

Methods

Fabrication of dense silver nanorod arrays

An optically thick (180 nm) silver film was deposited on a quartz substrate with a 6 nm titanium adhesion layer by electron-beam evaporation. Prior to the film deposition, the substrate was cleaned with acetone followed by deionized water and blown dry with a nitrogen gun. To minimize the roughness introduced by deposition, a low evaporation rate was employed (less than $0.05~\text{nm s}^{-1}$). Both titanium and silver films were deposited sequentially on the quartz substrate using an Edwards Auto 306 electron-beam evaporator at a base pressure of about 2×10^{-7} mbar. Negative resist NEB 22 of around 320 nm thickness was selected as the ion milling mask after EBL patterning and development. The area of each array was $\sim 8 \times 8~\mu\text{m}^2$. During ion milling (INTLVAC NANOQUEST), argon ions impinged upon the sample surface at an angle of 10°. The beam voltage was 300 V with 45 V accelerating voltage and 110 mA beam

[a]College of Information Science and Engineering, Northeastern University, Shenyang 110004, China

[b]Department of Engineering Science and Mechanics, The Pennsylvania State University, University Park, PA 16802, USA

[c]Department of Electrical and Computer Engineering, National University of Singapore, 4 Engineering Drive 3, Singapore 117576. E-mail: adanner@nus.edu.sg

[d]Institute of Materials Research and Engineering, Agency for Science, Technology and Research (A*STAR), 3 Research Link, Singapore 117602. E-mail: jh-teng@imre.a-star.edu.sg; liuy@imre.a-star.edu.sg

† These authors contributed equally to this work.

current. The total milling time was around 4 minutes with the power stabilized around 156 W. Resist residue was removed by Microposit Remover 1165 after ion milling.

Optical characterization

The optical response of the fabricated nanorods was measured using a UV-Vis-NIR microspectrometer (CRAIC QDI 2010™) at normal incidence with a 75 W broadband xenon source. We used a reflecting objective (magnification: 36×; numerical aperture: 0.5) to shine the white light onto the samples and collect the reflected light to both spectrometer and colored CCD simultaneously. The detecting area was limited to 7.1×7.1 μm^2 using a variable aperture. Reflection and transmission measurements were normalized with respect to an aluminium mirror and a bare quartz substrate, respectively.

FDTD simulations

Finite-difference time-domain (FDTD) simulations were performed using Lumerical packages.[43] The dispersion model of silver is based on data from Johnson and Christy[44] in the material library of the software. The simulation model was built based on the schematic shown in Fig. 1. One set of four silver nanorods was modelled with thickness ranging from 140 nm to 180 nm, providing a good agreement with experimental results. Note that the 6 nm titanium layer was also taken into account in our simulations. The dimension of the simulation area was set so as to allow two periods of the nanorod structure in the x–y plane and enough space for the light source and power monitors. Auto-nonuniform meshing with the finest meshes (0.25 nm minimum mesh step) was used to achieve the most accurate results. The auto-cutoff was set at 1×10^{-6} to ensure the convergence of the obtained results. Simulation time was set as 1000 μs with a step of 0.015 μs. The results usually

converged before the simulation time ran out. The light source covered wavelengths ranging from 300 nm to 1300 nm with an increasing step of 2 nm. A power monitor was located 300 nm above the silver rods and 100 nm above the light source to collect reflected and scattered modes reaching the detecting region.

Results and discussion

Fig. 1 illustrates the schematic view of the optical setup to characterize a reflective plasmonic color filter. Silver nanorod arrays with different periodicities were fabricated on a quartz substrate using standard EBL (Elionix ELS-7000) processes followed by ion milling. Fig. 2a is the scanning electron microscope (SEM) image of a representative sample with the structural parameters: periodicity $p = 550$ nm in both x- and y-directions (see Fig. 1), rod diameter $d = 275$ nm ($d/p = 0.5$), and height $h = 180$ nm. Fig. 2b plots the measured reflection spectra of nanorod arrays with large inter-rod gaps ($s \geq 200$ nm) and varying periodicities from 400 nm ($d = 200$ nm) to 700 nm ($d = 350$ nm) in 50 nm increments (i.e., the d/p ratio was kept constant at 0.5). As can be seen from Fig. 2b, the reflection spectra can be tuned across the near infrared range with various array periodicities. A shift in resonance peaks from 750 nm to 1270 nm is observed when the periodicity is increased from 400 nm to 700 nm. The reflected intensity varies within 10% and the full-width at half-maximum (FWHM) decreases noticeably at smaller periodicities. Fig. 2c plots the simulated reflection spectra based on the experimentally achieved structural data using the FDTD method. There are obvious differences between measurements and simulations (see Fig. 2b and c): experimental results show that the main resonance peaks become broader and show lower reflectance with increased periodicity; while simulations show that the FWHM remains almost constant and that reflectance becomes greater. These differences could be attributed to larger scattering in experiments compared to simulations, which causes broader FWHM and lower reflectance with increased periodicity. The larger scattering effect may arise from: (1) shape difference between the simulation model (perfect cylindrical rod) and the real sample (dome-like profile and non-circle shape); (2) surface oxidation of silver nanorods;[45,46] (3) nonuniform silver materials properties caused by different grain sizes and distribution during metal deposition. Nevertheless, the simulation results show qualitative agreement with experiments and thus confirm our design concept.

Complex mechanisms are involved when periodical plasmonic nanorod arrays are illuminated with light, including localized surface plasmon resonance (LSPR), Wood's anomalies and Bloch wave surface plasmon polaritons.[47] The collective plasmonic resonances at different wavelengths are the combined results of all three effects and their mutual coupling. LSPR can be estimated using the coupling dipole theory, which has been developed and discussed comprehensively elsewhere.[48,49] Each single rod can be modelled by a dipole of polarizability α, which can be written as:[50]
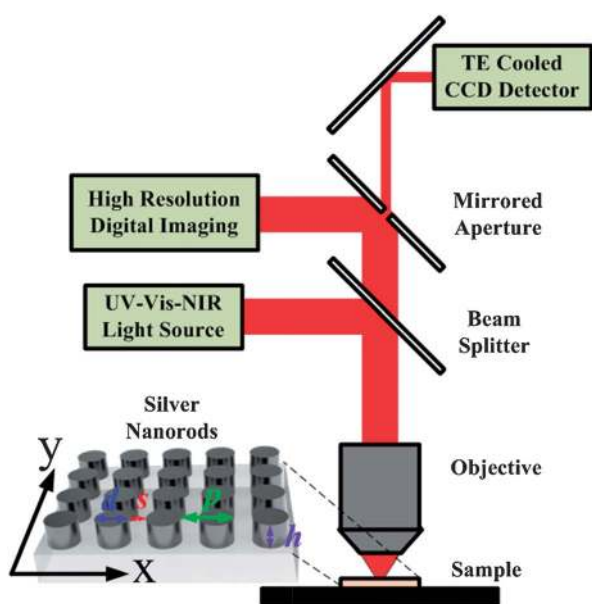

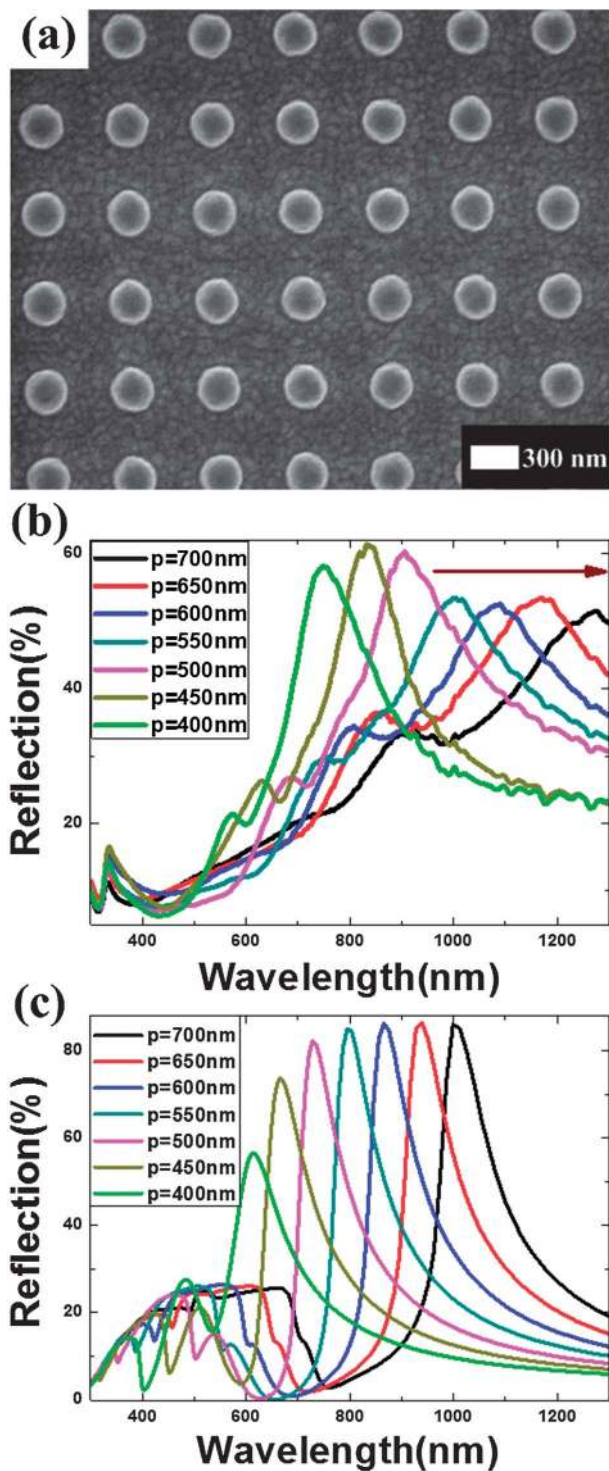**Fig. 1** Schematic diagram of the color filter working in reflection mode.

Fig. 2 (a) SEM image showing the top view of a silver nanorod array with period $p = 550$ nm. (b) Measured and (c) calculated reflection spectra for nanorod arrays with periodicities from 400 nm to 700 nm. The arrow indicates increasing periodicities.

$$\alpha^{\text{static}} \propto V \frac{\varepsilon_{\text{m}} - \varepsilon_{\text{d}}}{3\varepsilon_{\text{m}} + 3\chi(\varepsilon_{\text{m}} - \varepsilon_{\text{d}})} \tag{1}$$

where ε_{m} and ε_{d} are the relative permittivities of metal and surrounding environment, respectively. χ is the shape factor

relating to the physical shape of the nanorod and V is the volume of the nanorod. When the nanorod array is excited by an electromagnetic field with frequency ω, the rod dipole will radiate a scattering field in proportion to its dipole moment. The total LSPR field with an effective polarizability α^* is a combined effect of the incident field and radiation from each individual nanorods, which can be expressed as:[50]

$$\alpha^* = \frac{1}{1/\alpha - S} \tag{2}$$

with the array factor S denoting the collective effect of all nanorods and depending only on the geometrical factors of the nanorods. The S factor for a square array of nanorods under normal incidence can be written as:[50]

$$S = \sum_{\text{dipoles}} e^{\text{i}kr} \left[\frac{(1 - \text{i}kr)(3\cos^2\theta - 1)}{r^3} + \frac{k^2\sin^2\theta}{r} \right] \tag{3}$$

A peak in the reflection spectrum can be achieved when the condition $S = 1/\alpha$ is satisfied, which is the theoretical basis upon which to build our color filter since designated wavelengths can be separated by varying the sizes and periods of nanorod arrays.

To further investigate the impact of inter-rod gaps on the optical response of nanorods, we calculate the reflections in the visible range for nanorod arrays with constant periodicity $p = 400$ nm and varying inter-rod gaps and diameter sizes, as shown in Fig. 3. The peak intensity increases with larger d/p values, which is caused by the reduced distance between adjacent nanorods. As the gap size decreases to several tens of nanometers, the converted surface plasmon waves from the incident light will not enter the structure because the ultrasmall gaps between nanorods allow nothing but zero plasmon modes,[51,52] which cannot penetrate the nanorod layers of 180 nm. Most of the waves will only exist at the interface of air/rods and will be decoupled back into propagating electromagnetic waves as the reflection towards the incident direction. Apart from the intrinsic absorption and the damping loss of the surface
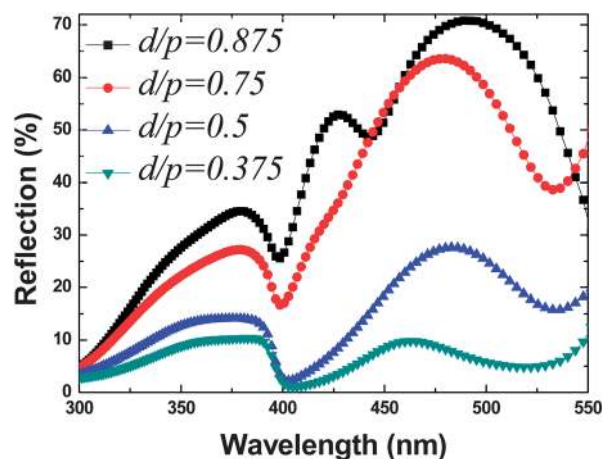

Fig. 3 Calculated reflection of nanorod arrays with constant periodicity $p = 400$ nm and varying inter-rod gaps and diameters corresponding to different d/p values ranging from 0.375 to 0.875.

plasmon waves, most of the input light energy reflects back as resonance peaks where the surface plasmon waves can be excited and the intensity will increase as the size of the gap decreases, which will be confirmed by the following experiments.

To experimentally demonstrate the reflection-mode color filter, we fabricated plasmonic color filters according to the design with different d/p values and dramatically decreased inter-rod gaps. SEM images of nanorods with different inter-rod gaps are shown in Fig. 4. The silver rods have been milled through and very small (20–40 nm) inter-rod gaps can be clearly observed. Using nanorods with different periodicities from 540 nm (Fig. 4a) to 320 nm (Fig. 4e) with a step size of 55 nm, we filtered individual colors out as shown in Fig. 5a. From the top view of the rods (Fig. 4f), ultrasmall inter-rod gap sizes (~25 nm) can be clearly observed. The structural parameters of the arrays are summarized in Table 1. As expected, strong optical excitations in the visible band of the spectrum are observed. By changing the periodicity of the nanorod arrays, tuning of the resonance peak wavelengths between 480 nm (blue) to 630 nm (red) is achieved, as shown in Fig. 5b. One can see that when the periodicity is 540 nm ($s = 40$ nm), a broad resonance is located at ~630 nm. When the periodicity is reduced to 485 nm ($s = 35$ nm), the resonance peak shifts to about 580 nm, exhibiting a yellow color. Furthermore, when the periodicity is smaller than 430 nm, narrower resonance peaks are distinct and more reflected energies are observed due to stronger coupling in the small cavities, displaying as green, cyan and blue, respectively. Note that more intensity is reflected as the periodicity is decreased. The relatively large FWHM of the curve for the blue

Fig. 5 (a) Optical image showing the reflective colors from different silver nanorod arrays. Measured reflection (b) and transmission (c) spectra of the corresponding arrays as a function of wavelengths.

color compared to other spectra is due to fabrication imperfections. Some of the rods are touching each other (see Fig. 4e). Once the conductive contact between rods is established, the original surface charge distribution is broken and a different regime is formed. The conductive coupling between nanorods leads to redistribution of surface charges, resulting in the mergence of separate individual modes. Fig. 5c presents the
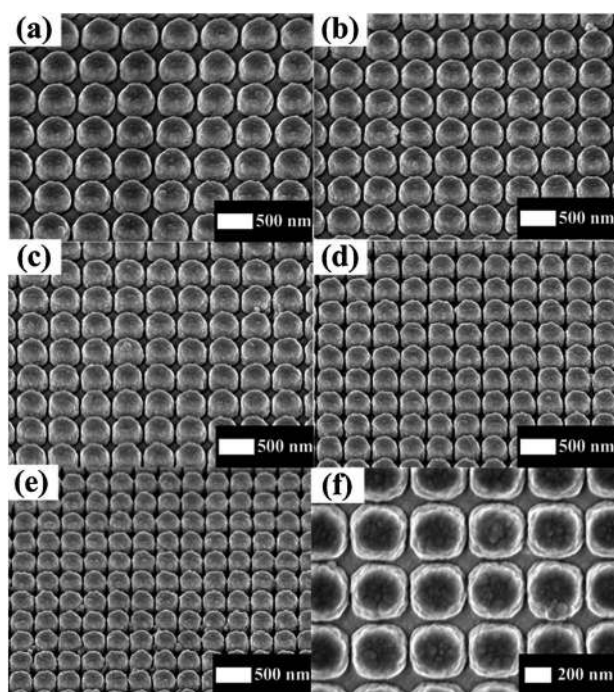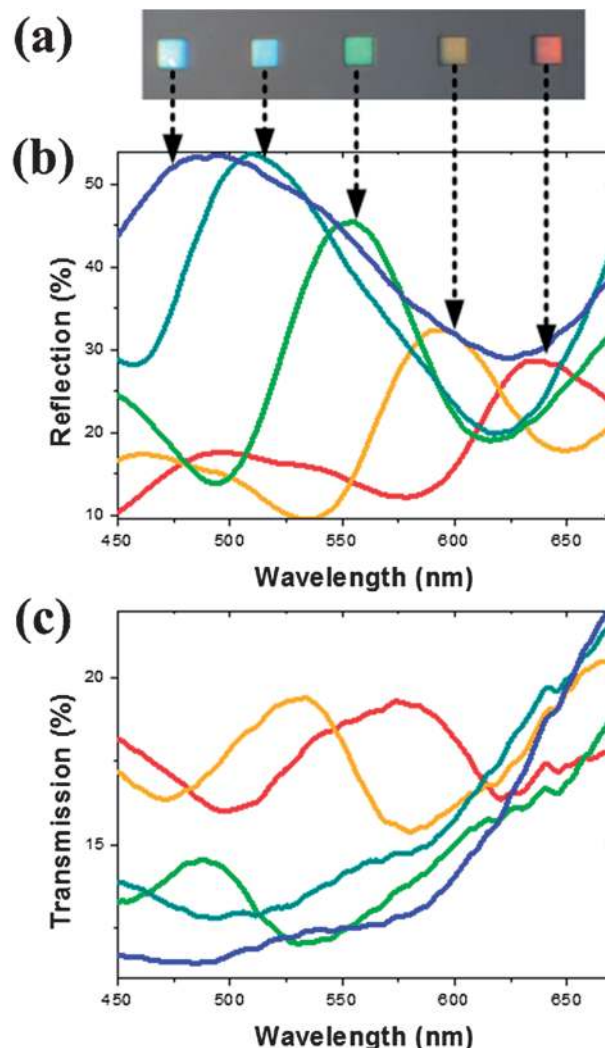

Fig. 4 SEM images showing oblique views of dense nanorod arrays with different periodicities from (a) 540 nm to (e) 320 nm with a step size of 55 nm. (f) Magnified top view of (d) with $p = 375$ nm and $d = 350$ nm.

Table 1 Optimized parameters of the nanorod arrays and the corresponding reflected colors

Presented color	Periodicity (nm)	Rod diameter (nm)	Gap (nm)	d/p
Red	540	500	40	0.926
Yellow	485	450	35	0.928
Green	430	400	30	0.930
Cyan	375	350	25	0.933
Blue	320	300	20	0.938

measured transmission spectra which show relatively low intensities (less than 20% in the visible range), leading to a high efficiency reflective color filter.

Conclusions

In summary, we have demonstrated tuning of the plasmon resonance using dense plasmonic nanorod arrays. The optical response depends strongly on the periodicity of the arrays and the diameter/periodicity ratio. Effective tuning of surface plasmon resonance peaks is achieved across the near infrared range using plasmonic nanorod arrays with inter-rod gaps larger than 200 nm. The reflection peaks coincide with the plasmon resonance and nanorod arrays with different periodicities can act as color filters suitable for reflection measurement. Individual colors are demonstrated by using dense plasmonic nanorods with ultrasmall inter-rod gaps smaller than 40 nm and different array periodicities. A variety of applications such as sensing, imaging and displays can be readily realized by varying either the geometry or the surrounding media of the nanorods.

Acknowledgements

Notes and references

1 H. J. Chen, Z. H. Sun, W. H. Ni, K. C. Woo, H.-Q. Lin, L. D. Sun, C. H. Yan and J. F. Wang, *Small*, 2009, **5**, 2111–2119.

2 X. S. Kou, Z. H. Sun, Z. Yang, H. J. Chen and J. F. Wang, *Langmuir*, 2009, **25**, 1692–1698.

3 X. Wu, T. Ming, X. Wang, P. N. Wang, J. F. Wang and J. Y. Chen, *ACS Nano*, 2010, **4**, 113–120.

4 J. B. Lassiter, H. Sobhani, J. A. Fan, J. Kundu, F. Capasso, P. Nordlander and N. J. Halas, *Nano Lett.*, 2010, **10**, 3184–3189.

5 J. A. Fan, C. Wu, K. Bao, J. Bao, R. Bardhan, N. J. Halas, V. N. Manoharan, P. Nordlander, G. Shvets and F. Capasso, *Science*, 2010, **328**, 1135–1138.

6 J. A. Fan, K. Bao, C. Wu, J. Bao, R. Bardhan, N. J. Halas, V. N. Manoharan, G. Shvets, P. Nordlander and F. Capasso, *Nano Lett.*, 2010, **10**, 4680–4685.

7 J. B. Lassiter, J. Aizpurua, L. I. Hernandez, D. W. Brandl, I. Romero, S. Lal, J. H. Hafner, P. Nordlander and N. J. Halas, *Nano Lett.*, 2008, **8**, 1212–1218.

8 R. Bardhan, N. K. Grady, T. Ali and N. J. Halas, *ACS Nano*, 2010, **4**, 6169–6179.

9 I. Zorić, E. M. Larsson, B. Kasemo and C. Langhammer, *Adv. Mater.*, 2010, **22**, 4628–4633.

10 C. Langhammer, M. Schwind, B. Kasemo and I. Zorić, *Nano Lett.*, 2008, **8**, 1461–1471.

11 Y. J. Liu, Y. B. Zheng, J. Liou, I.-K. Chiang, I. C. Khoo and T. J. Huang, *J. Phys. Chem. C*, 2011, **115**, 7717–7722.

12 T. W. Ebbesen, H. J. Lezec, H. F. Ghaemi, T. Thio and P. A. Wolff, *Nature*, 1998, **391**, 667–669.

13 Y. J. Liu, E. S. P. Leong, B. Wang and J. H. Teng, *Plasmonics*, 2011, **6**, 659–664.

14 P. Nordlander, *ACS Nano*, 2009, **3**, 488–492.

15 A. R. Halpern and R. M. Corn, *ACS Nano*, 2013, **7**, 1755–1762.

16 H. J. Chen, L. Shao, Q. Li and J. F. Wang, *Chem. Soc. Rev.*, 2013, **42**, 2679–2724.

17 Y. D. Zheng, M. D. Xiao, S. X. Jiang, F. Ding and J. F. Wang, *Nanoscale*, 2013, **5**, 788–795.

18 G. A. Wurtz, R. Pollard, W. Hendren, G. P. Wiederrecht, D. J. Gosztola, V. A. Podolskiy and A. V. Zayats, *Nat. Nanotechnol.*, 2011, **6**, 107–111.

19 G. A. Wurtz, W. Dickson, D. O'Connor, R. Atkinson, W. Hendren, P. Evans, R. Pollard and A. V. Zayats, *Opt. Express*, 2008, **16**, 7460–7470.

20 D. P. Lyvers, J. M. Moon, A. V. Kildishev, V. M. Shalaev and A. Wei, *ACS Nano*, 2008, **2**, 2569–2576.

21 A. M. Kern and O. J. F. Martin, *Nano Lett.*, 2011, **11**, 482–487.

22 J. P. Kottmann, O. J. F. Martin, D. R. Smith and S. Schultz, *Opt. Express*, 2000, **6**, 213–219.

23 A. Lovera and O. J. F. Martin, *Appl. Phys. Lett.*, 2011, **99**, 151104.

24 J. A. Dionne, K. Diest, L. A. Sweatlock and H. A. Atwater, *Nano Lett.*, 2009, **9**, 897–902.

25 M. J. Dicken, L. A. Sweatlock, D. Pacifici, H. J. Lezec, K. Bhattacharya and H. A. Atwater, *Nano Lett.*, 2008, **8**, 4048–4052.

26 Y. J. Liu, Q. Hao, J. S. T. Smalley, J. Liou, I. C. Khoo and T. J. Huang, *Appl. Phys. Lett.*, 2010, **97**, 091101.

27 R. A. Pala, K. T. Shimizu, N. A. Melosh and M. L. Brongersma, *Nano Lett.*, 2008, **8**, 1506–1510.

28 X. Zhang, H. Liu, J. Tian, Y. Song and L. Wang, *Nano Lett.*, 2008, **8**, 2653–2658.

29 Y. Zhao, M. A. Belkin and A. Alù, *Nat. Commun.*, 2012, **3**, 870.

30 N. Liu, M. Mesch, T. Weiss, M. Hentschel and H. Giessen, *Nano Lett.*, 2010, **10**, 2342–2348.

31 Y. Wang, T. Sun, T. Paudel, Y. Zhang, Z. Ren and K. Kempa, *Nano Lett.*, 2012, **12**, 440–445.

32 K. Aydin, V. E. Ferry, R. M. Briggs and H. A. Atwater, *Nat. Commun.*, 2011, **2**, 517.

33 Y. Zhao, Q. Hao, Y. Ma, M. Lu, B. Zhang, M. Lapsley, I. C. Khoo and T. J. Huang, *Appl. Phys. Lett.*, 2012, **100**, 053119.

34 E. Laux, C. Genet, T. Skauli and T. W. Ebbesen, *Nat. Photonics*, 2008, **2**, 161–164.

35 W. Cai, U. K. Chettiar, H. K. Yuan, V. C. de Silva, A. V. Kildishev, V. P. Drachev and V. M. Shalaev, *Opt. Express*, 2007, **15**, 3333–3341.

36 T. Xu, Y. K. Wu, X. G. Luo and L. J. Guo, *Nat. Commun.*, 2010, **1**, 59.

37 G. Y. Si, Y. H. Zhao, H. Liu, S. L. Teo, M. S. Zhang, T. J. Huang, A. J. Danner and J. H. Teng, *Appl. Phys. Lett.*, 2011, **99**, 033105.

38 Y. J. Liu, G. Y. Si, E. S. P. Leong, B. Wang, A. J. Danner, X. C. Yuan and J. H. Teng, *Appl. Phys. A: Mater. Sci. Process.*, 2012, **107**, 49–54.

39 Y. J. Liu, G. Y. Si, E. S. P. Leong, N. Xiang, A. J. Danner and J. H. Teng, *Adv. Mater.*, 2012, **24**, OP131–OP135.

40 J. Zhang, J. Ou, N. Papasimakis, Y. Chen, K. F. MacDonald and N. I. Zheludev, *Opt. Express*, 2011, **19**, 23279–23285.

41 K. Kumar, H. Duan, R. S. Hegde, S. C. W. Koh, J. N. Wei and J. K. W. Yang, *Nat. Nanotechnol.*, 2012, **7**, 557–561.

42 G. Y. Si, Y. H. Zhao, J. T. Lv, F. W. Wang, H. L. Liu, J. H. Teng and Y. J. Liu, *Nanoscale*, **5**, 4309–4313.

43 Lumerical FDTD solution: http://www.lumerical.com/.

44 P. B. Johnson and R. W. Christy, *Phys. Rev. B: Solid State*, 1972, **6**, 4370–4379.

45 E. S. P. Leong, Y. J. Liu, B. Wang and J. H. Teng, *ACS Appl. Mater. Interfaces*, 2011, **3**, 1148–1153.

46 E. S. P. Leong, Y. J. Liu, C. C. Chum and J. H. Teng, *Plasmonics*, 2013, **8**, 1221–1226.

47 K. Lee and P. Wei, *Small*, 2010, **6**, 1900–1907.

48 S. Zou and G. C. Schatz, *Nanotechnology*, 2006, **17**, 2813–2820.

49 V. A. Markel and A. K. Sarychev, *Phys. Rev. B: Condens. Matter Mater. Phys.*, 2007, **75**, 085426.

50 B. Auguié and W. L. Barnes, *Phys. Rev. Lett.*, 2008, **101**, 143902.

51 M. J. Levene, J. Korlach, S. W. Turner, M. Foquet, H. G. Craighead and W. W. Webb, *Science*, 2003, **299**, 682–686.

52 M. Foquet, K. T. Samiee, X. Kong, B. P. Chauduri, P. M. Lundquist, S. W. Turner, J. Freudenthal and D. B. Roitman, *J. Appl. Phys.*, 2008, **103**, 034301.